

Multimodal CARS microscopy of structured carbohydrate biopolymers

Aaron D. Slepko,^{1,*} Andrew Ridsdale,¹ Adrian F. Pegoraro,^{1,2}
Douglas J. Moffatt,¹ and Albert Stolow^{1,2}

¹Steacie Institute for Molecular Sciences, National Research Council of Canada, Ottawa,
Ontario, K1A 0R6 Canada

²Department of Physics, Queen's University, Kingston, Ontario, K7L 3N6 Canada
*aaron.slepko@nrc.gc.ca

Abstract: We demonstrate the utility of multimodal coherent anti-Stokes Raman scattering (CARS) microscopy for the study of structured condensed carbohydrate systems. Simultaneous second-harmonic generation (SHG) and spectrally-scanned CARS microscopy was used to elucidate structure, alignment, and density in cellulose cotton fibers and in starch grains undergoing rapid heat-moisture swelling. Our results suggest that CARS response of the O-H stretch region (3000 cm^{-1} – 3400 cm^{-1}), together with the commonly-measured C-H stretch (2750 cm^{-1} – 2970 cm^{-1}) and SHG provide potentially important structural information and contrast in these materials.

©2010 Optical Society of America

OCIS codes: (180.4315) Nonlinear microscopy; (300.6230) Spectroscopy, coherent anti-Stokes Raman scattering; (160.1435) Biomaterials.

References and links

1. A. Zumbusch, G. R. Holtom, and X. S. Xie, "Three-dimensional vibrational imaging by coherent anti-Stokes Raman scattering," *Phys. Rev. Lett.* **82**(20), 4142–4145 (1999).
2. J.-X. Cheng, and X. Xie, "Coherent anti-Stokes Raman scattering microscopy: Instrumentation, theory, and applications," *J. Phys. Chem. B* **108**(3), 827–840 (2004).
3. C. L. Evans, and X. S. Xie, "Coherent anti-stokes Raman scattering microscopy: chemical imaging for biology and medicine," *Annu Rev Anal Chem (Palo Alto Calif)* **1**(1), 883–909 (2008).
4. B. von Vacano, T. Buckup, and M. Motzkus, "Highly sensitive single-beam heterodyne coherent anti-Stokes Raman scattering," *Opt. Lett.* **31**(16), 2495–2497 (2006).
5. A. F. Pegoraro, A. D. Slepko, A. Ridsdale, J. P. Pezacki, and A. Stolow, "Single laser source for multimodal coherent anti-Stokes Raman scattering microscopy," *Appl. Opt.* **49**(25), F10–F17 (2010).
6. A. Volkmer, "Coherent Raman Scattering Microscopy", in *Emerging Raman Applications and Techniques in Biomedical and Pharmaceutical Fields*, P. Matousek and M. D. Morris, Eds. (Springer, New York, 2010).
7. M. Müller, and J. M. Schins, "Imaging the thermodynamic state of lipid membranes with multiplex CARS microscopy," *J. Phys. Chem. B* **106**(14), 3715–3723 (2002).
8. J.-X. Cheng, A. Volkmer, L. D. Book, and X. S. Xie, "Multiplex coherent anti-stokes Raman scattering microspectroscopy and study of lipid vesicles," *J. Phys. Chem. B* **106**(34), 8493–8498 (2002).
9. E. O. Potma, and X. S. Xie, "Detection of single lipid bilayers with coherent anti-Stokes Raman scattering (CARS) microscopy," *J. Raman Spectrosc.* **34**(9), 642–650 (2003).
10. H. Wang, Y. Fu, P. Zickmund, R. Shi, and J.-X. Cheng, "Coherent anti-stokes Raman scattering imaging of axonal myelin in live spinal tissues," *Biophys. J.* **89**(1), 581–591 (2005).
11. T. Hellerer, C. Axäng, C. Brackmann, P. Hillertz, M. Pilon, and A. Enejder, "Monitoring of lipid storage in *Caenorhabditis elegans* using coherent anti-Stokes Raman scattering (CARS) microscopy," *Proc. Natl. Acad. Sci. U.S.A.* **104**(37), 14658–14663 (2007).
12. R. K. Lyn, D. C. Kennedy, S. M. Sagan, D. R. Blais, Y. Rouleau, A. F. Pegoraro, X. S. Xie, A. Stolow, and J. P. Pezacki, "Direct imaging of the disruption of hepatitis C virus replication complexes by inhibitors of lipid metabolism," *Virology* **394**(1), 130–142 (2009).
13. J.-X. Cheng, L. D. Book, and X. S. Xie, "Polarization coherent anti-Stokes Raman scattering microscopy," *Opt. Lett.* **26**(17), 1341–1343 (2001).
14. C. W. Freudiger, W. Min, B. G. Saar, S. Lu, G. R. Holtom, C. He, J. C. Tsai, J. X. Kang, and X. S. Xie, "Label-free biomedical imaging with high sensitivity by stimulated Raman scattering microscopy," *Science* **322**(5909), 1857–1861 (2008).
15. H. Wang, Y. Fu, P. Zickmund, R. Shi, and J.-X. Cheng, "Coherent anti-stokes Raman scattering imaging of axonal myelin in live spinal tissues," *Biophys. J.* **89**(1), 581–591 (2005).

16. R. S. Lim, A. Kratzer, N. P. Barry, S. Miyazaki-Anzai, M. Miyazaki, W. W. Mantulin, M. Levi, E. O. Potma, and B. J. Tromberg, "Multimodal CARS microscopy determination of the impact of diet on macrophage infiltration and lipid accumulation on plaque formation in ApoE-deficient mice," *J. Lipid Res.* **51**(7), 1729–1737 (2010).
17. L. B. Mostaço-Guidolin, M. G. Sowa, A. Ridsdale, A. F. Pegoraro, M. S. D. Smith, M. D. Hewko, E. K. Kohlenberg, B. Schattka, M. Shiomu, A. Stolow, and A. C.-T. Ko, "Differentiating atherosclerotic plaque burden in arterial tissues using femtosecond CARS-based multimodal nonlinear optical imaging," *Biomed. Opt. Express* **1**(1), 59–73 (2010).
18. T. Hellerer, A. M. K. Enejder, and A. Zumbusch, "Spectral focusing: high spectral resolution spectroscopy with broad-bandwidth laser pulses," *Appl. Phys. Lett.* **85**, 25 (2004).
19. A. F. Pegoraro, A. Ridsdale, D. J. Moffatt, Y. Jia, J. P. Pezacki, and A. Stolow, "Optimally chirped multimodal CARS microscopy based on a single Ti:sapphire oscillator," *Opt. Express* **17**(4), 2984–2996 (2009).
20. Y. Fu, T. B. Huff, H.-W. Wang, J.-X. Cheng, and H. Wang, "Ex vivo and in vivo imaging of myelin fibers in mouse brain by coherent anti-Stokes Raman scattering microscopy," *Opt. Express* **16**(24), 19396–19409 (2008).
21. H.-W. Wang, T. T. Le, and J.-X. Cheng, "Label-free imaging of arterial cells and extracellular matrix using a multimodal CARS microscope," *Opt. Commun.* **281**(7), 1813–1822 (2008).
22. X. Nan, E. O. Potma, and X. S. Xie, "Nonperturbative chemical imaging of organelle transport in living cells with coherent anti-stokes Raman scattering microscopy," *Biophys. J.* **91**(2), 728–735 (2006).
23. C. P. Pfeffer, B. R. Olsen, F. Ganikhanov, and F. Légaré, "Multimodal nonlinear optical imaging of collagen arrays," *J. Struct. Biol.* **164**(1), 140–145 (2008).
24. F. John, Robyt, *Essentials of Carbohydrate Chemistry* (Springer-Verlag, 1998), Chap. 6.
25. A. Buléon, G. Véronèse, and J.-L. Putaux, "Self-association and crystallization of amylose," *Aust. J. Chem.* **60**(10), 706–718 (2007).
26. A. Buléon, and P. Colonna, "Physicochemical Behaviour of Starch in Food Applications", in *The Chemical Physics of Food*, P. Belton, ed. (Blackwell Publishing Ltd, Oxford, 2007).
27. C. G. Biliaderis, "The structure and interactions of starch with food constituents," *Can. J. Physiol. Pharmacol.* **69**(1), 60–78 (1991).
28. T. Loftsson, and D. Duchêne, "Cyclodextrins and their pharmaceutical applications," *Int. J. Pharm.* **329**(1–2), 1–11 (2007).
29. A. Gunaratne, and R. Hoover, "Effect of heat-moisture treatment on the structure and physicochemical properties of tuber and root starches," *Carbohydr. Polym.* **49**(4), 425–437 (2002).
30. H. F. Zobel, "Molecules to Granules: A Comprehensive Starch Review," *Starch* **40** 44–50 (1988).
31. P. M. Fechner, S. Wartewig, P. Kleinebudde, and R. H. Neubert, "Studies of the retrogradation process for various starch gels using Raman spectroscopy," *Carbohydr. Res.* **340**(16), 2563–2568 (2005).
32. G. Cox, N. Moreno, and J. Feijó, "Second-harmonic imaging of plant polysaccharides," *J. Biomed. Opt.* **10**(2), 024013 (2005).
33. K. N. Anisha Thayil, E. J. Gualda, S. Psilodimitrakopoulos, I. G. Cormack, I. Amat-Roldán, M. Mathew, D. Artigas, and P. Loza-Alvarez, "Starch-based backwards SHG for in situ MEFISTO pulse characterization in multiphoton microscopy," *J. Microsc.* **230**(1), 70–75 (2008).
34. R. Cisek, L. Spencer, N. Prent, D. Zigmantas, G. S. Espie, and V. Barzda, "Optical microscopy in photosynthesis," *Photosynth. Res.* **102**(2–3), 111–141 (2009).
35. R. Carriles, D. N. Schafer, K. E. Sheetz, J. J. Field, R. Cisek, V. Barzda, A. W. Sylvester, and J. A. Squier, "Invited review article: Imaging techniques for harmonic and multiphoton absorption fluorescence microscopy," *Rev. Sci. Instrum.* **80**(8), 081101 (2009).
36. S. Psilodimitrakopoulos, I. Amat-Roldán, P. Loza-Alvarez, and D. Artigas, "Estimating the helical pitch angle of amylopectin in starch using polarization second harmonic generation microscopy," *J. Opt.* **12**(8), 084007 (2010).
37. Z.-Y. Zhuo, C.-S. Liao, C.-H. Huang, J.-Y. Yu, Y.-Y. Tzeng, W. Lo, C.-Y. Dong, H.-C. Chui, Y.-C. Huang, H.-M. Lai, and S.-W. Chu, "Second harmonic generation imaging - a new method for unraveling molecular information of starch," *J. Struct. Biol.* **171**(1), 88–94 (2010).
38. R. Cisek, A. Tuer, S. Krouglov, I. J. Tetlow, F. Liu and V. Barzda, University of Toronto Mississauga, are preparing a manuscript titled "Harmonic generation microscopy of starch granules."
39. <http://www.britannica.com/EBchecked/topic/101633/cellulose>; accessed September 9, 2010.
40. P. Zugenmaier, *Crystalline Cellulose and Cellulose Derivatives* (Springer, Berlin, 2008).
41. R. H. Atalla and D. L. Vanderhart, "Studies on the structure of cellulose using Raman spectroscopy and solid state C NMR," ICP Technical Paper Series no. 306 (1988), pp. 1–20.
42. J. H. Wiley, and R. H. Atalla, "Band assignments in the Raman-spectra of celluloses," *Carbohydr. Res.* **160**, 113–129 (1987).
43. M. E. Himmel, S. Y. Ding, D. K. Johnson, W. S. Adney, M. R. Nimlos, J. W. Brady, and T. D. Foust, "Biomass recalcitrance: engineering plants and enzymes for biofuels production," *Science* **315**(5813), 804–807 (2007).
44. T. T. Teeri, "Crystalline cellulose degradation: new insight into the function of cellobiohydrolases," *Trends Biotechnol.* **15**(5), 160–167 (1997).
45. D. Klemm, B. Heublein, H. P. Fink, and A. Bohn, "Cellulose: fascinating biopolymer and sustainable raw material," *Angew. Chem. Int. Ed. Engl.* **44**(22), 3358–3393 (2005).
46. Y. Marubashi, T. Higashi, S. Hirakawa, S. Tani, T. Erata, M. Takai, and J. Kawamata, "Second Harmonic Generation Measurements for Biomacromolecules: Celluloses," *Opt. Rev.* **11**(6), 385–387 (2004).
47. R. M. J. Brown, Jr., A. C. Millard, and P. J. Campagnola, "Macromolecular structure of cellulose studied by second-harmonic generation imaging microscopy," *Opt. Lett.* **28**(22), 2207–2209 (2003).
48. O. Nadiarnykh, R. B. Lacombe, P. J. Campagnola, and W. A. Mohler, "Coherent and incoherent SHG in fibrillar cellulose matrices," *Opt. Express* **15**(6), 3348–3360 (2007).

49. M. Åkerholm, B. Hinterstoisser, and L. Salmén, "Characterization of the crystalline structure of cellulose using static and dynamic FT-IR spectroscopy," *Carbohydr. Res.* **339**(3), 569–578 (2004).
50. B. Bakri, and S. J. Eichhorn, "Elastic coils: deformation micromechanics of coir and celery fibres," *Cellulose* **17**(1), 1–11 (2010).
51. M. Zimmerley, R. Younger, T. Valenton, D. C. Oertel, J. L. Ward, and E. O. Potma, "Molecular orientation in dry and hydrated cellulose fibers: a coherent anti-Stokes Raman scattering microscopy study," *J. Phys. Chem. B* **114**(31), 10200–10208 (2010).
52. A. D. Slepkov, A. Ridsdale, H.-N. Wan, M.-H. Wang, A. F. Pegoraro, D. J. Moffatt, J. P. Pezacki, F.-J. Kao, and A. Stolow, "Forward-Collected FLIM-CARS Microscopy," *J. Biomed. Opt.* In press.
53. D. J. Gallant, B. Bouchet, and P. M. Baldwin, "Microscopy of starch: evidence of a new level of granule organization," *Carbohydr. Polym.* **32**(3–4), 177–191 (1997).
54. <http://www.chemistryexplained.com/Pl-Pr/Polymers-Natural.html>, accessed September 2010.
55. N. Gierlinger, S. Luss, C. König, J. Konnerth, M. Eder, and P. Fratzl, "Cellulose microfibril orientation of Picea abies and its variability at the micron-level determined by Raman imaging," *J. Exp. Bot.* **61**(2), 587–595 (2010).
56. B. Hinterstoisser, M. Åkerholm, and L. Salmén, "Effect of fiber orientation in dynamic FTIR study on native cellulose," *Carbohydr. Res.* **334**(1), 27–37 (2001).

1. Introduction

Coherent anti-Stokes Raman scattering (CARS) microscopy has garnered widespread interest as a label-free and chemically-specific nonlinear optical imaging modality [1–3]. Because CARS signal intensity typically scales as the concentration squared [4] of Raman-active bonds in the sample, CARS microscopy is best suited for studying condensed and aggregated materials. As such, while ever-growing in utility within the biomedical imaging community [3,5,6], CARS microscopy has developed a reputation as predominantly a lipid-imaging modality [7–12]. There have been several recent advances that attempt to overcome this intrinsic concentration obstacle to allow imaging of dilute species and enable imaging in the "fingerprint" region of biological samples, either within the traditional CARS framework [4,13], or by using other Raman sensitive techniques [14]. For many applications, however, CARS lipid imaging can offer significant insight when combined with other nonlinear optical imaging techniques for true multimodal imaging [15–17].

Our approach to multimodal CARS imaging utilizes high-bandwidth femtosecond pulses combined with "spectral focusing" [18] in order to provide a very simple platform that readily integrates with other nonlinear microscopy techniques such as second harmonic generation (SHG) and two-photon excitation fluorescence (TPEF). This approach also permits rapid spectral scanning and improved spectral resolution over conventional fs-based CARS microscopy [5,19]. The implementation of spectral focusing significantly improves the contrast of resonant-to-nonresonant signals [19], while the ability to rapidly obtain the CARS spectrum in an imaging modality (so called hyper-spectral imaging) allows for chemical-specificity via vibrational fingerprinting [19]. Multimodal CARS imaging systems have been used to study lipid rich systems such as myelin [15,20], atherosclerotic tissues [17,21], and lipid droplets in live cells [12,22], as well as non-lipid based systems rich in C-H vibrations such as collagen arrays [23].

These studies need not be limited to lipid structures, however, particularly when CARS imaging is simultaneously combined with other structure-sensitive imaging modalities such as SHG. Carbohydrate polymers such as starch, cellulose, and glycogen are condensed biomaterials that present a wide array of structures and functions. Members of this family of naturally occurring sugar-based polymers are extremely similar in chemical composition. Different polymer linkages, modes of bio-synthesis, and hydrogen-bonding structure give rise to materials with differing properties and biological and technological functionalities [24]. By combining spectral-scanning CARS microscopy with other nonlinear optical imaging modalities, it is possible to offer insight into the structure as well as the dynamics of these materials.

The structure, composition, and physio-chemical properties of starch grains are topics of active research and are of significant interest to the food science [25–27], and pharmacological [28] industries. Starch is a glucose polymer often found in plants in the form of grains. Starch grains are water insoluble complex networks of amylose and amylopectin which form layered crystalline and amorphous domains [25,29]. Of particular interest to

starch research is the dynamical process of grain swelling and retrograding that occurs when starch grains are heat-treated in excess water [27,29]. Traditionally, structure in native and retrograded starch is studied by x-ray diffraction, calorimetry, light scattering, and Raman spectroscopy [30,31]. Most of these techniques require long-timescale analysis of the initial and final products. We find that—like lipids—starch grains provide very strong CARS signals in the C-H vibrational region (2750 cm^{-1} – 2970 cm^{-1}). However, unlike lipids, there is additionally a strong CARS signal in the O-H region (3000 cm^{-1} – 3400 cm^{-1}). Furthermore, starches provide strong SHG signals [32–35], and recent research demonstrates the intimate connection between polarization-resolved SHG signals and the crystalline structure of different types of starch grains [36–38]. The concurrent combination of SHG and CARS microscopies presented herein yields complementary information on both internal structure and bond density. As opposed to spontaneous Raman scattering microscopy, CARS imaging is sufficiently fast to allow real-time visualization of starch grain swelling under rapid heat-moisture treatment. We present movies ([Media 1](#)) of this process with simultaneous SHG and CARS modalities in order to demonstrate the potential utility of multimodal CARS microscopy for starch research applications.

Cellulose—the most abundant naturally occurring organic material on earth [39]—is compositionally identical to starch (specifically, amylose and amylopectin) with the only difference being that the glucose units are linked via acetal beta-linkages, as opposed to alpha-linkages. This polymerization geometry leads to a significantly more linear chain that incorporates strong inter- and intra-molecular hydrogen bonding [40–42]. As a consequence, unlike starch, cellulose is indigestible by most mammals. Like starch grains, native cellulose is a highly organized biomaterial that displays a variety of crystal structures which determine physical properties [40]. The microscopic structure and micro-fibril alignment within both native and modified (or synthetic) cellulose fibers is a subject of active research with applications in biofuels [43], textiles and paper [44,45], and high-performance materials industries [45], to name a few.

Studies of cellulose structure also traditionally utilize x-ray diffraction. Recently, there has been considerable interest in utilizing SHG [46–48], and vibrational spectroscopies such as FTIR [49] and Raman [42,50] for studying the structure and mechanical properties of cellulose fibers and films. A recent study demonstrated the potential of CARS microscopy for examining local structure in native and synthetic cellulose fibers [51]. In that study, the authors utilized a new polarization-based analysis of the CARS response of cotton and rayon fibers in order to map out local structure using the CARS signal ratio of symmetric and asymmetric C-H stretch vibrations (at 2890 cm^{-1} and 2963 cm^{-1} , respectively). Here, we demonstrate that in addition to the strong CARS signal in the C-H region, there is a strong and spectrally-structured signal within the O-H region of the spectrum that is known to arise primarily from inter-molecular hydrogen bonding in cellulose fibers [41] and which can be used to image local structural inhomogeneity. The (2850 cm^{-1} – 3400 cm^{-1}) CARS signals from cellulose and starch represent molecular fingerprints which are distinct from each other as well as from lipid systems which have minimal resonant response in the O-H vibration spectral region and enable us to perform microspectroscopy on these important materials.

2. Materials and methods

A schematic of the experimental optical layout is shown in Fig. 1. A Mira 900 Ti:Sapphire oscillator outputs 60 fs pulses of 795 nm light at an 80-MHz repetition rate. This beam is divided on a variable beamsplitter to send 150-200 mW to a commercially-mounted microstructured fiber (NKT Photonics, FemtoWhite CARS) for supercontinuum generation. We typically obtain 33% transmission through the fiber. The supercontinuum is filtered with a set of long-pass filters ($\lambda > 950\text{ nm}$) to provide the Stokes beam for CARS imaging. The remainder of the Ti:Sapphire laser power is sent to a computer-controlled delay stage and a variable attenuator (half-wave plate and polarizer combination), en-route to a dichroic beam combiner (Chroma Technology cdxr950) where it is combined with the Stokes pulses. The

beams are then routed to a laser-scanning inverted microscope (Olympus FV300) which has been modified for collection of non-descanned light in the forward direction using a multimode optical fiber, as described elsewhere [52]. An Olympus 40X 1.15 N.A. UAPO water immersion lens with a cover slip correction is used for imaging. The forward directed signal is filtered by a 700 nm short-pass filter to eliminate the excitation pulses and the remaining CARS (~650 nm) and SHG (~400 nm) signals are separated using a dichroic mirror and each sent to individual PMT detectors, as depicted in Fig. 1. The mismatch between the 1.15 NA objective and 0.55 NA condenser reduces overall SHG throughput but does not appear to reduce contrast or distort the images.

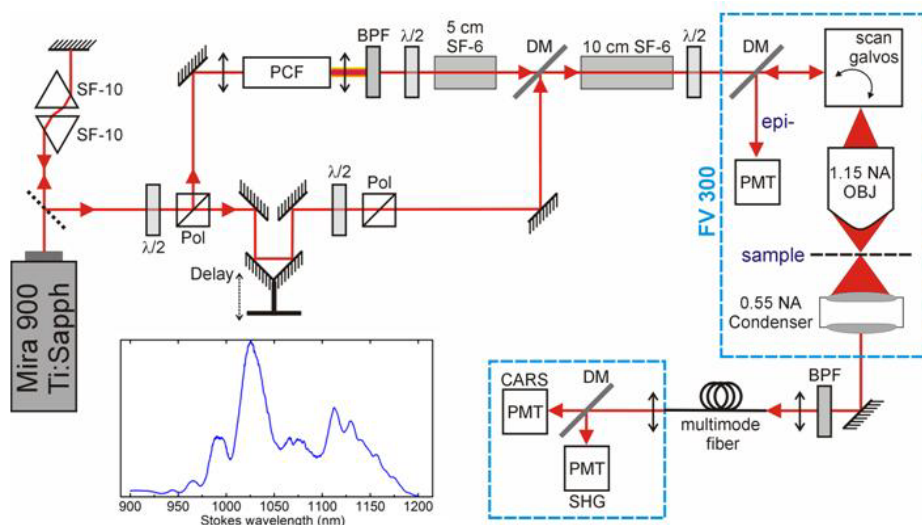


Fig. 1. Femtosecond single-source multimodal CARS microscopy optical layout: Pulses from a Ti:Sapphire oscillator are sent through a prism compressor before being split by a variable beam splitter. One arm is sent through a photonic crystal fiber (PCF) where it generates a broadband supercontinuum Stokes light. This beam then passes to a long-pass ($\lambda > 900$ nm) filter (LPF) and a 5-cm-long block of SF-6 before being recombined on a dichroic mirror (DM). The other beam is sent through a time delay arm and a variable attenuator. The two beams are recombined and then pass through an additional 10-cm of SF-6 glass before being routed into an Olympus FV300 microscope. The forward-propagating CARS and SHG signals are separated from the excitation pulses with a long-pass ($\lambda < 700$ nm, SPF) filter (SPF), collected in a non-descanned geometry through a multimode fiber and are routed to off-board detectors. Pol: polarizer; $\lambda/2$: half-wave plate; OBJ: objective; PMT: photomultiplier tubes. A sample Stokes continuum spectrum entering the microscope is provided in the inset.

As previously reported [19], our single-femtosecond-laser-source CARS microscope relies on matching chirp rates (spectral focusing) of the pump and Stokes pulses for optimal CARS signal level and spectral resolution. We simply and effectively implement spectral focusing [18] in our microscope system by the addition of a 5-cm-long anti-reflection-coated block of SF-6 glass in the Stokes arm and an additional 10-cm-long block in the joint arm, as shown in Fig. 1. This scheme significantly improves spectral resolution and improves contrast between the resonant signal and nonresonant background. Furthermore, the probed Raman frequency can be rapidly scanned by continuous adjustment of the time-overlap of the two pulses using a computer-controlled delay stage on the pump arm. For imaging the aliphatic C-H stretch band at ~ 2900 cm^{-1} , we temporally overlap the 795-nm pump pulse with the 1033-nm component of the broadband Stokes spectrum at the focus of the objective, generating an anti-Stokes pulse at 646 nm. Likewise, for imaging the O-H stretch band at ~ 3200 cm^{-1} , the pump pulses are overlapped temporally with the 1066-nm Stokes component, generating an anti-Stokes pulse at 634 nm. In practice, the delay stage scans continuously to overlap the pump pulses through the entire temporal (and hence spectral) range of the Stokes pulses to yield the CARS

spectrum. The CARS signal varies linearly with the instantaneous Stokes power and quadratically with the pump power. Concurrent with the two-beam CARS response, a SHG signal is collected in the forward direction, and is quadratically proportional to the pump power. For joint SHG and CARS imaging, we introduce 7-9 mW of total (>950 nm) Stokes power and 30-200 mW of pump power into the laser-scanning unit and microscope. Ultimately, the incident Stokes power at the sample focus is approximately 300 μ W. The amount of pump power used depends on the application and the brightness of the image; 130 mW of pump was typically used for the experiments presented in this article. The pump polarization is set with a half-wave plate at the entrance to the microscope, and the Stokes polarization is set with respect to the pump with a half-wave plate after the supercontinuum generation fiber. For the CARS studies presented here, the Stokes polarization was aligned parallel to that of the pump.

In the following, we present images from potato and rice starch grains and from cellulose fibers suspended in either deuterated- or tap-water. Potato starch was extracted from home-grown potatoes by suspending freshly-cut cubes in room-temperature water with intermittent agitation for an hour. The starch grains rapidly settle to the bottom where they can be aspirated with a pipette, transferred to a sample vial, and washed several times in clean tap water. For starch grains from rice (premium short-grain sushi rice), several grains of rice were crushed between two pieces of glass, and then suspended in a small volume of water to extract some starch in the same manner as described for potato. Sample preparation of starch grains for heat-moisture treatment involved placing a drop of a dilute starch-water suspension on a sapphire microscope coverslip and allowing the water to evaporate overnight in a flow-hood. The sample, now largely adherent to the coverslip, is then re-wetted with the desired surrounding medium and covered with a concavity microscope slide. This procedure sufficiently fixes the grains to the coverslip and minimizes the chances that a given observed grain will drift in the suspension while imaging. For heat-moisture swelling studies, the prepared slides are placed onto an inverted Peltier microscope temperature control stage (Linkam Co., UK). Thermal contact is made between the stage and sapphire coverslip with a small film of index-matching oil. The stage temperature can be regulated between -5°C and 100°C . Movies ([Media 1](#)) of starch grain swelling in water were taken during a steady temperature increase at the sample location. The stage temperature was set to ramp up quickly to the 80°C setting, held there for several minutes, and then slowly raised ($1^{\circ}\text{C}/\text{min}$) to the 90°C setting. No attempt was made to determine the precise temperature at the sample location. Starch grains are known to undergo rapid swelling between 59°C - 65°C [29–31].

Cellulose samples were obtained by extracting a few strands of cotton from Puritan brand laboratory cotton swabs and mounting them in the desired surrounding liquid between a coverslip and a flat glass microscope slide.

3. Results and discussion

3.1 CARS and SHG microscopy of starch

Potato starch grains are composed of approximately 65% amylopectin and 20% amylose, with 15% water and 0.1% lipids [30]. Macroscopically, the grain is composed of striated hard crystalline and soft semi-crystalline layers of amylopectin that radiate outwards from the central hilum core [53]. While the crystalline structure of the grain itself is macroscopically centro-symmetric, within the crystalline layers, the amylopectin chains are strongly anisotropically aligned within the focal volume of the laser and thus yield a strong second-order nonlinear optical response. The semi-crystalline layers, however, are not expected to generate SHG signals. The utility of SHG microscopy for the study of starch grains is a current topic of research interest [32–38]. The implementation of CARS with SHG imaging of starch grains provides complimentary information. Unlike SHG, which is primarily a probe of crystalline structure [36], CARS signal is largely a probe of the resonant bond concentration, and thus of local density. The combined SHG and CARS signals (C-H stretch at 2880 cm^{-1}) of potato starch grains are shown in Fig. 2(a). The CARS signal is brighter than the second-

harmonic signal and yields excellent contrast with the background water. In the CARS image, the aforementioned striations are clearly visible, as is the hilum which appears as a dark “dimple” in the grain. These striations are also somewhat visible in the SHG overlay, but to a lesser extent. Interestingly, it is observed that the bright striations in the SHG image appear to

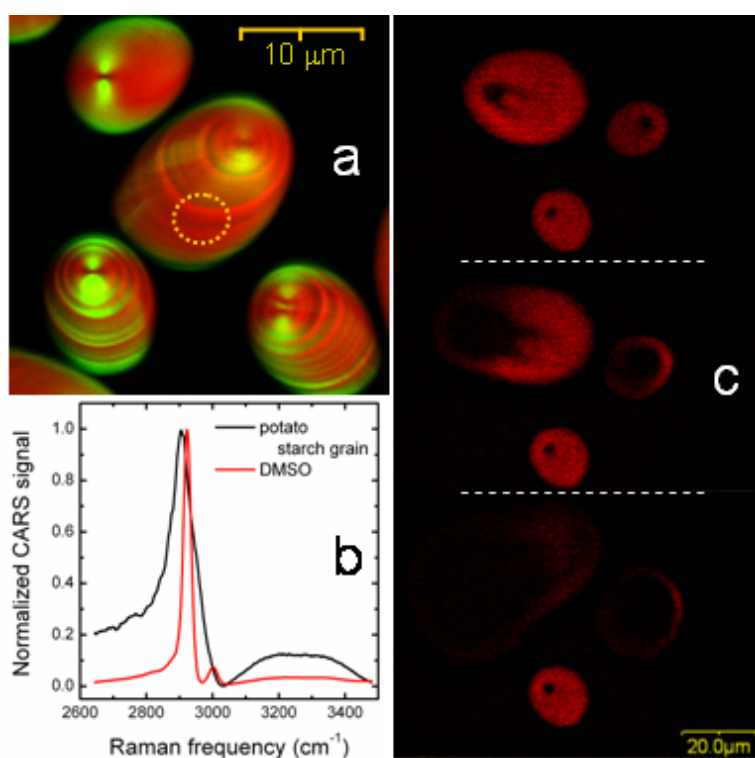


Fig. 2. Potato starch grains. (a) Overlaid CARS (red) and SHG (green) images of potato starch grains in which striations associated with alternating crystalline and amorphous layers are clearly visible and appear to be anti-correlated between SHG and CARS. The pump and Stokes beams are polarized in the vertical direction. The 512×512 pixel image represents a Kalman average of 5 scans, acquired in a total of 5 seconds. (b) Nonresonant-background normalized CARS spectrum of starch sampled from the region of interest outlined in yellow in (a), and shown together with a representative spectrum for DMSO for comparison. (c) Start, middle, and end frames from a movie of a potato starch grain swelling upon heating in excess water (Media 1). Elapsed time between the first and last frames is approximately 150 seconds.

be largely anti-correlated with the bright striations in the CARS image. Because the CARS response is sensitive to small variations in concentration and the SHG signal is mainly sensitive to crystallinity, these preliminary results suggest that crystalline layers in the grain are less dense than the amorphous layers. To our knowledge, this is the first such indication in the literature, but more experiments are necessary to verify this hypothesis. Alternative explanations are that the striations seen in the CARS image are mainly due to greater scattering from the crystalline layers, or that the birefringence in the crystalline layers is highly dispersive (in wavelength) and thus rotates the relative polarization alignment of the Stokes and pump beams, diminishing the CARS signal [13].

The nonresonant-background-normalized CARS spectrum from an arbitrary region of interest (ROI) in one grain is shown next to the CARS spectrum obtained from a reference dimethyl sulfoxide (DMSO) sample in Fig. 2(b). The DMSO spectrum is shown in order to indicate the excellent spectral resolution of our femtosecond-CARS microscope as well as to show the difference between the CARS spectrum of a typical hydrocarbon and that of starch. In particular, starch displays a well-resolved broad band in the O-H stretch region, from 3100

cm^{-1} to 3500 cm^{-1} . We observed no differences in the CARS spectra between the dark and bright striation regions.

In Fig. 2(c), we show three frames from a 1.7 frame per second video ([Media 1](#)) of potato starch swelling in water under heating conditions. The rapid drop-off of CARS signal with reduced concentration is evident as water penetrates the grain, and thereby reduces the C-H bond density of the crystalline material. As the grain is seen to swell, it presents a growing void of CARS signal. Notably, the grain does not dissolve in water from the outside in, but rather, water penetrates the grain and “melts” the structure from the inside out. This behavior is even more apparent when considering the combined SHG and CARS signals. In Fig. 3(a) we present frames from a movie ([Media 2](#)) of a rapidly-swelling rice starch grain in water. Here, the SHG signal is seen to diminish much faster than the CARS signal, indicating that the structure inside the grain is disrupted faster than the reduction in density due to swelling. Spectral CARS scans taken at the end of the movie confirm that the fully-swollen grain is still surrounded by an intact starch periphery which is significantly denser than in the center, as shown in Fig. 3(b). Nonetheless, crystallinity in this grain appears to have disappeared, as indicated by the absence of any SHG signal.

The precise dynamical process by which starch grains swell is an active and contentious area of research. Studies have identified nanoscopic pores and channels that span the outer layers of starch grains and are hypothesized to participate in the inflow of water (and outflow of amylose) during swelling [53]. These nanoscopic channels are beyond the resolution of a light microscope. However, the ability to study dynamic changes in the density and structure of starch grains *during* the process of swelling provides a clear indication of the strong potential impact multimodal CARS microscopy can have on the field of starch research. For example, in all potato starch-grain heat-moisture courses that we have observed to date, swelling is seen to initiate in the vicinity of the hilum, rather than strictly in the center of the grain. This is clearly observable in Fig. 2(c) and its associated movie ([Media 1](#)).

3.2 CARS and SHG microscopy of cellulose

Cotton fibers represent the purest natural form of cellulose [54]. Microscopically, cellulose fibers are composed of crystalline nanometer-scale fibrils interspersed with regions of non-crystalline cellulose chains. Natural cellulose has two similar crystallization structures, known as cellulose I_{α} and cellulose I_{β} [40]. The relative ratio of these two forms changes depending on fiber origin. Cotton is mainly comprised of cellulose I_{β} . The main difference between these two crystal structures lies in the intra-molecular hydrogen bonding pattern [40–42]. Thus, these two structures present slightly different Raman spectra in the O-H region (3000 cm^{-1} - 3400 cm^{-1}), and this fingerprint has been used as a main identification tool to distinguish between the two [41]. Similarly, CARS microscopy may be utilized for such fingerprinting, while SHG can simultaneously monitor local structure and level of crystallinity.

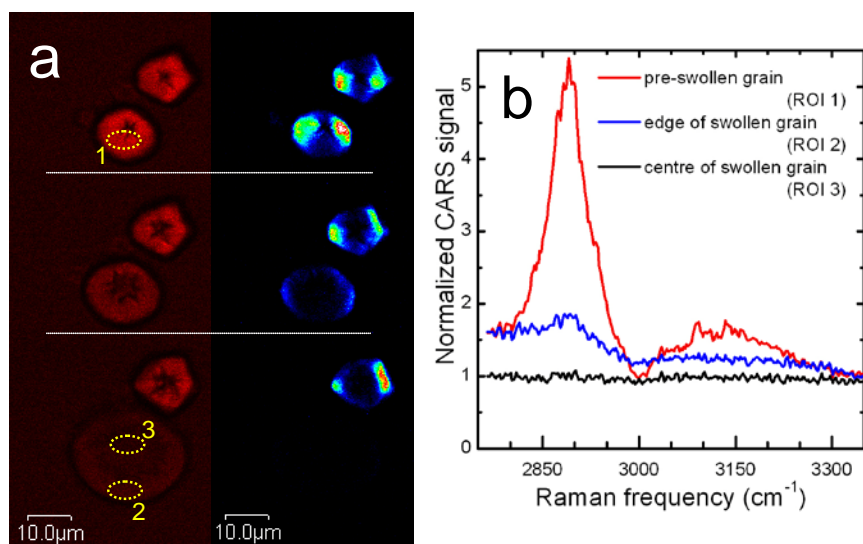


Fig. 3. Rice starch grain swelling. (a) Start, middle, and end frames from a movie of a rice starch grain swelling upon heating in excess water (Media 2). CARS and SHG images are shown side-by-side on the left and right, respectively. The color-scheme for SHG is chosen to emphasize contrast (blue-to-red-to-white; low-to-high). Disappearance of SHG signal is seen long before disappearance of the CARS signal, strongly suggesting that crystallinity is reduced before the bulk dilution of starch (swelling) takes place. Elapsed time between the first and last frames is approximately 150 seconds. (b) CARS spectra taken before the onset of swelling (from ROI 1 in (a)) and after swelling (from ROI 2 and 3 in (a)), indicating that the swollen grain is intact and still surrounded by a diluted starch layer. The spectra in ROI 1, 2, and 3 are normalized to the spectra from the surrounding water (not shown).

Simultaneous CARS and SHG microscopy images of a cotton fiber in water are presented in Fig. 4(a). Similar to the case with starch grains, the bright CARS signal is observed to be more uniform over the entire strand compared to the SHG image which is more directly sensitive to microscopic crystalline structure. In the case of SHG, the non-uniformity of the image mostly arises from the use of linear polarized excitation and the SHG image would appear more uniform if circular-polarized excitation were used (which would detrimentally impact the simultaneously-collected CARS intensity). The CARS spectrum, taken from an arbitrary ROI and compared to that from an adjacent ROI in the surrounding water, is strongly peaked at both the C-H region near 2900 cm^{-1} and at the O-H stretch at 3220 cm^{-1} . In addition to these main peaks, there is a secondary, much smaller C-H stretch feature at 2960 cm^{-1} and a second O-H peak at 3300 cm^{-1} , as shown in Fig. 4(b). Very recently, Zimmerley *et al.* [51] showed that, as in spontaneous Raman spectroscopic studies [55], a CARS polarization analysis can prove sensitive to anisotropy and orientation of the polyglucan chains in natural and synthetic cellulose fibers. Furthermore, they suggest that local changes in the ratio of the two C-H stretch peaks (identified at 2890 cm^{-1} and 2963 cm^{-1} in [51]) are associated with structural changes and inter-molecular alignment in cotton fibers.

We find that the local changes in the O-H peaks are distinct from those of the C-H region, as might be expected from the fact that the C-H stretch arises mainly from intra-molecular structure, while the identified O-H stretch peaks are also associated with inter-molecular hydrogen bonding structure [40–42]. This is demonstrated in Fig. 5. Figs. 5(a) and 5(b) show a segment of cotton fiber in D_2O imaged by CARS (at 2900 cm^{-1}) and SHG, respectively. As expected, considerably more structure is seen in the SHG image compared to that of the CARS image taken at a single vibrational frequency. Comparing the CARS spectrum across the image, however, indicates a considerably higher level of structural non-uniformity elucidated by this method. This is evident from the spectra shown in Fig. 5(c) taken from the two ROI indicated in Fig. 5(a). These have very different $2900/2960\text{ cm}^{-1}$ and

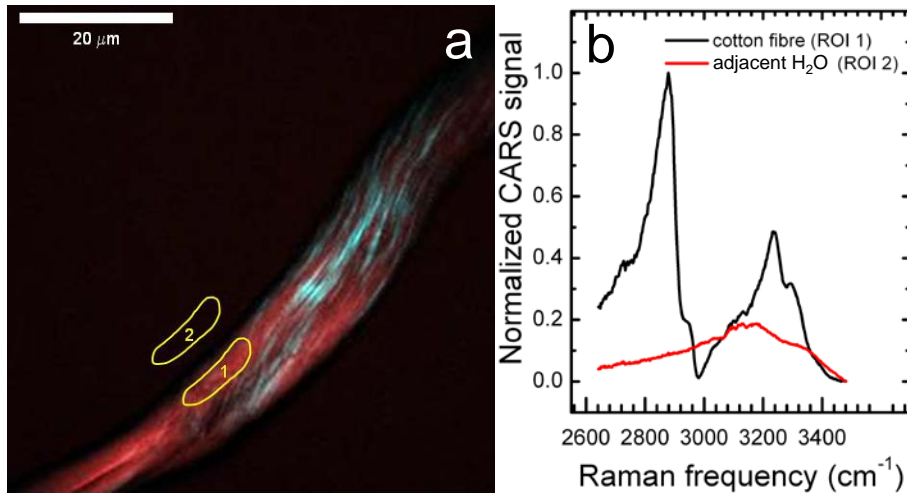


Fig. 4. CARS and SHG from a cotton fiber in water. (a) The CARS signal (red) illuminates the fiber more uniformly than does the striped SHG signal (cyan). The Stokes and pump beams are aligned vertically with respect to the image. (b) Representative CARS spectra of cellulose and background water are taken from the ROIs in (a). The O-H stretch region in cotton cellulose is clearly distinct from the broad and mostly featureless O-H region in water.

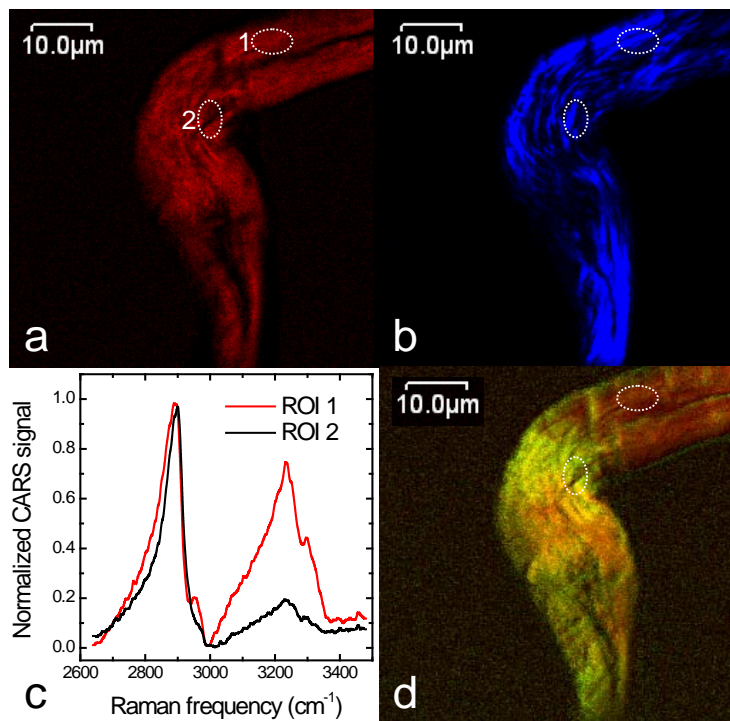


Fig. 5. CARS and SHG from a cotton fiber in deuterated water. (a) A CARS image taken at 2900 cm^{-1} . The Stokes and pump beams are aligned vertically with respect to the image. (b) Simultaneously-obtained SHG image. (c) CARS spectra from the two ROI indicated in (a), showing clear differences in the relative signal intensities at the C-H and O-H stretch regions. (d) An overlay map of the ratio of the pixel-by-pixel CARS signals at $2900/2960\text{ cm}^{-1}$ (red) and $2900/3220\text{ cm}^{-1}$ (green). The colourmaps scale such that an average ratio of 1 is background and a ratio of 4.3 is maximum intensity in the green channel and a ratio of 12.6 is maximum in the red channel. The average value in the red channel over ROI 1 is 4.5.

2900/3220 cm^{-1} CARS signal ratios. An overlay map of these two ratios is presented in Fig. 5(d). This figure contains considerably more structural contrast than that found in the single CARS frequency image (Fig. 5(a)). Furthermore, it can be seen that the two signal ratios vary across the fiber, and thus represent distinct measures of structure in these fibers. In particular, it is observed that the relative strength of O-H stretch signal diminishes markedly at the sharp bend. This indicates a local disruption in inter-chain hydrogen bonding that may be due to stress/strain-induced structural changes [56]. We clearly identify gross positionally-varying changes in the CARS spectra in these samples. However, as shown by Zimmerly *et al.* [51], the birefringent nature of cotton fibers necessitates full polarization control and analysis in ascribing local spectral changes to structural orientations. Thus, the combination of polarization-resolution and CARS spectral imaging in the CH and OH regions will prove a powerful tool for future studies structured biopolymer assemblies.

4. Summary

We have identified a strong CARS response in common carbohydrate polymers such as starch and cellulose, and have shown that, together with the commonly-measured C-H stretch (2750 cm^{-1} – 2970 cm^{-1}), the O-H stretch region (3000 cm^{-1} – 3400 cm^{-1}) is an important source of structural-information and image contrast in these materials. We showed that our experimental scheme comprising of a single femtosecond laser-source and associated supercontinuum Stokes source allows for rapid scanning of the CARS spectrum and for simple simultaneous SHG and CARS imaging. Together, these complimentary nonlinear imaging modalities provide both information on local bond density and structural orientation. Their joint use shows considerable potential for the study of condensed carbohydrate polymer systems. The addition of concurrently-obtained TPEF signal is easily implemented, but as the samples under consideration for this article show only small levels of endogenous fluorescence, these images have not been included. We are currently expanding this research to the study of glycogen in live cells and tissues, and to the elucidation of starch degradation and retrogradation process during heat-moisture swelling. It is also of interest to investigate the apparent anti-correlation between the CARS and SHG signals in striated starch grains, and the disruption in hydrogen-bonding that occurs at kinks/bends in cellulose fibers.

Acknowledgments

The authors would like to acknowledge Virginijus Barzda of the University of Toronto Mississauga for fruitful discussions. This research was largely funded by a joint NRC-NSC-ITRI Canada-Taiwan Cooperation project “Digital FLIM-CARS Microscopy.”